Exchange interactions of $CaMnO_3$ in the bulk and at the surface

S. Keshavarz,[1] Y. O. Kvashnin,[1] D. C. M. Rodrigues,[1,2] M. Pereiro,[1] I. Di Marco,[1] C. Autieri,[1] L. Nordström,[1] I. V. Solovyev,[3,4] B. Sanyal,[1] and O. Eriksson[1]

[1]*Uppsala University, Department of Physics and Astronomy, Division of Materials Theory, Box 516, SE-751 20 Uppsala, Sweden*

[2]*Faculdade de Física, Universidade Federal do Pará, CEP 66075-110, Belém, Pará, Brazil*

[3]*National Institute for Materials Science, 1-1 Namiki, Tsukuba, Ibaraki 305-0044, Japan*

[4]*Department of Theoretical Physics and Applied Mathematics, Ural Federal University, Mira Street 19, 620002 Ekaterinburg, Russia*

(Received 25 October 2016; revised manuscript received 18 January 2017; published 10 March 2017; publisher error corrected 1 June 2018)

We present electronic and magnetic properties of $CaMnO_3$ (CMO) as obtained from *ab initio* calculations. We identify the preferable magnetic order by means of density functional theory plus Hubbard U calculations and extract the effective exchange parameters (J_{ij}'s) using the magnetic force theorem. We find that the effects of geometrical relaxation at the surface as well as the change of crystal field are very strong and are able to influence the lower-energy magnetic configuration. In particular, our analysis reveals that the exchange interaction between the Mn atoms belonging to the surface and the subsurface layers is very sensitive to the structural changes. An earlier study [A. Filippetti and W. E. Pickett, Phys. Rev. Lett. **83**, 4184 (1999)] suggested that this coupling is ferromagnetic and gives rise to the spin-flip (SF) process on the surface of CMO. In our work, we confirm their finding for an unrelaxed geometry, but once the structural relaxations are taken into account, this exchange coupling changes its sign. Thus, we suggest that the surface of CMO should have the same G-type antiferromagnetic order as in the bulk. Finally, we show that the suggested SF can be induced in the system by introducing an excess of electrons.

DOI: 10.1103/PhysRevB.95.115120

I. INTRODUCTION

Magnetic transition-metal (TM) perovskites are a fascinating class of materials, exhibiting a sophisticated interplay between structure, charge, orbital and spin degrees of freedom [1]. As a result, depending on their composition, they exhibit a variety of different ordered states and possess various useful physical properties, such as multiferroicity [2,3], noncollinear magnetism [4], half metallicity, and colossal magnetoresistance (CMR) (see, e.g., Ref. [5]), which make these materials attractive for spintronic applications. Nowadays, very clean surfaces and sharp interfaces between different perovskites can be synthesised with great precision. Exotic phenomena such as superconductivity [6] and a realization of two-dimensional (2D) electron gas [7,8] have been reported for 2D-derived perovskite materials. This technological advancement boosted not only the experimental investigations in this direction, but also led to many fundamental questions for theory.

One of the fundamental questions for magnetic TM perovskites is as follows: How does a system react microscopically when it is confined to two dimensions? A lower symmetry and a reduced coordination number change the electronic structure and therefore all related properties. Due to the above-mentioned coexistence of several degrees of freedom, these changes are difficult to predict in TM perovskites and first-principles electronic structure calculations are necessary. Among perovskite systems, the mixed-valence manganites are of particular interest [5,9–11].

The present study concerns a classical TM oxide: $CaMnO_3$ (CMO). In bulk, the sixfold-coordinated Mn ions form a set of half-filled t_{2g} orbitals, corresponding to the formal valence state Mn^{4+}. Strongly antiferromagnetic (AFM) superexchange interactions [12] between these ions give rise to a G-type AFM order, which is stabilized below the Néel point of 120 K [13,14].

However, at the surface of CMO, the Mn ions are surrounded by only five oxygen atoms. This dramatically changes the electronic structure, since the less bonded Mn e_g states shift to the low-energy region and form the metallic bands at the Fermi level. In this case, the ferromagnetic (FM) double-exchange mechanism [15–17] comes into play, competing with the superexchange coupling. Hence the interatomic exchange interactions (J_{ij}'s) at the surface of CMO will be defined by the subtle balance between these two contributions, and are therefore expected to be very different from the bulk values.

Filippetti and Pickett [18] investigated the surface of CMO by means of density functional theory (DFT). The authors considered a slab of six-layer thickness, analyzed its band structure, and calculated several magnetic configurations. They found that the surface and subsurface Mn spins are coupled ferromagnetically through a double-exchange-type mechanism. This change of sign of the exchange interaction results in a magnetic reconstruction at the surface of CMO, where the surface spins reverse their orientations, i.e., undergo a spin-flip (SF) process.

In the present study, we reexamine the electronic and magnetic structure of the surface of CMO in the presence of strong on-site correlation effects between 3d electrons. The calculations are based on a combination of DFT plus a static mean-field approach (DFT+U) [19]. The preferable magnetic order is identified by direct total-energy comparison, as well as by extracting the J_{ij}'s through the magnetic force theorem. We also point out the importance of structural relaxation effects at the surface and their influence on the exchange interactions.

This paper is organized as follows. Computational details are presented in Sec. II. Section III is devoted to our results, illustrated in several sections. First the magnetic properties of bulk CMO are presented; next we discuss the results of the slab calculation with and without geometrical relaxation. For all considered cases, we identify the preferable magnetic order

and analyze in detail the J_{ij}'s in the system. We also discuss the possibility of modifying the magnetic order on the surface of CMO by adding a uniform electron doping. Finally, our conclusions are illustrated in Sec. IV.

II. COMPUTATIONAL DETAILS

Bulk CMO crystallizes in the orthorhombic perovskite structure having *Pnma* space group with the lattice parameters $a = 5.28$ Å, $b = 0.99a$, and c $= \sqrt{2}a$ [14]. In this structure, the Mn-O-Mn angle is 158° rather than 180° as in the ideal perovskite structure. This structure was taken as the starting point for all of the calculations performed in this work. For the surface simulations, we have used a supercell geometry consisting of six alternating layers of CaO mediated and terminated by seven layers of MnO_2 stacked along the (001) direction. Since the periodic boundary conditions are used in all of the three dimensions, a 20-Å-thick layer of vacuum is used in the construction of the supercell.

We first performed a full structural relaxation of both bulk and slabs by means of the the projector augmented wave method [20], as implemented in the VASP code [21]. The plane-wave energy cutoff was set to 550 eV and the forces were converged up to 0.01 eV/Å. The k integration over the Brillouin zone was performed using $7 \times 7 \times 5$ points for bulk and $7 \times 7 \times 1$ points for the slabs. We first performed a set of calculations using the local spin density approximation (LSDA) [22], following Refs. [18,23]. Then, to improve the treatment of the localized TM $3d$ electrons, we performed additional calculations using the LSDA+U [19] approach. The Coulomb interaction parameters, the Hubbard U and Hund exchange J, were previously estimated by Hong *et al.* [24] by fitting energy differences of LSDA+U for different U values to those obtained from hybrid-functional energy, for the same electronic structure. In this way, they estimated $U - J = 3$ eV. Therefore, we used $U = 4$ eV and $J = 0.9$ eV, in agreement with other studies [25,26]. The double counting (DC) was considered in the fully localized limit (FLL) [27] both for bulk and surface, since it gives a proper description of several experimental properties.

The optimal structure was then used as input for electronic structure calculations through the full-potential linear muffin-tin orbital (FP-LMTO) code RSPt [28], in the scalar relativistic approximation. LSDA+U was considered in the most general formulation, with a four-index Coulomb interaction matrix constructed from the parameters U and J. The details of this implementation can be found in Refs. [28–31]. The converged electronic structure calculations were then used to calculate the interatomic exchange parameters. This is achieved by mapping the magnetic excitations onto the Heisenberg Hamiltonian:

$$\hat{H} = -\sum_{i \neq j} J_{ij} \vec{e}_i \cdot \vec{e}_j, \tag{1}$$

where J_{ij} is an exchange interaction between the two spins, located at sites i and j, and $\vec{e}_i$ is a unit vector along the magnetization direction at the corresponding site. In this work, the pairwise exchange parameters were obtained by means of the magnetic force theorem [32]. The set of local orbitals belonging to a given site was constructed by means of the so-called muffin-tin heads, as discussed in detail, together with other technical issues, in Ref. [33].

Finally, we used the extracted J_{ij}'s to calculate the ordering temperature of bulk CMO by means of a classical Monte Carlo (MC) algorithm for the solution of the Heisenberg Hamiltonian [Eq. (1)], as implemented in the UPPASD code [34]. In the recent past, a similar procedure was found to describe well the ordering temperatures of several elements and compounds, e.g., bcc Fe [34], hcp Gd [35], Heusler alloys [36], and transition-metal oxides [37]. Despite these results, we should note that, in principle, the extracted J_{ij}'s depend on the electronic structure. Therefore, the values derived in the ordered magnetic states at $T = 0$ cannot be generally used in the region near the ordering temperature, where there is a substantial magnetic disorder. However, if the main mechanism in the system is the superexchange, such as in the bulk of CMO, the J_{ij}'s do not depend on the magnetic state in which they are calculated using the magnetic force theorem, such as in MnO [38], $YTiO_3$ [39], and $MnWO_4$ [40]. In this case, it is theoretically sound to derive the J_{ij}'s in the ordered magnetic ground state and then to use them for the evaluation of the Néel temperature using, e.g., the classical MC method.

III. RESULTS AND DISCUSSIONS

A. Bulk of $CaMnO_3$

As experimentally and theoretically reported, CMO in bulk form is a G-type antiferromagnet [41,42]. This means that both intra- and interplane coupling between the Mn atoms are antiferromagnetic. Based on this knowledge, we performed the simulations for bulk CMO considering only G-AFM order. In Fig. 1, the total density of states (DOS) is presented. As expected, LSDA+U leads to a larger band gap than plain LSDA. Due to the distortion of the MnO_6 octahedra, the cubic degeneracies of the d orbitals are lifted. However, the splitting between the states is small and, therefore, we can still classify the electronic states as e_g-like and t_{2g}-like orbitals. With this definition in mind, we observe that the gap is opened between the t_{2g} (d_{xz},d_{xy},d_{yz}) and e_g (d_{xy},d_{z^2}) states below and above E_F, respectively. Therefore, this material can be classified as a Mott insulator according to the Zaanen-Sawatzky-Allen diagram [43]. The value of the band gap is found to be 0.4 and 1.1 eV in LSDA and LSDA+U, respectively. The band gap in LSDA is in close agreement with the results from earlier electronic structure calculations [18,44], while the band gap in LSDA+U is in fair agreement with the experimental optical band gap (1.55 eV) according to Ref. [13].

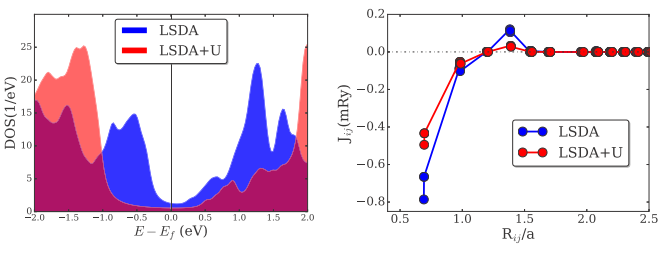

FIG. 1. Total DOS (left panel) and exchange parameters between Mn atoms (right panel) in bulk CMO.

Further insight into the magnetic structure can be obtained by calculating the exchange parameters J_{ij}, reported in Fig. 1(b). Negative values indicate AFM couplings. The points around $R_{ij}/a = 1/\sqrt{2}$ are considered to be the first nearest neighbors (NN), which are different due to structural distortion. The exchange parameters with the first NN are the strongest ones and are found to be AFM, which confirms the G-type AFM order for this system as the ground state in both LSDA and LSDA+U methods. It is interesting to observe that for bulk CMO, the J_{ij}'s extracted from LSDA+U are relatively suppressed compared to those of LSDA. This can be understood from the fact that the dominating exchange mechanism in TM oxides is the superexchange. The latter is proportional to $t^2/\Delta_{s.f.}$ (see, e.g., [47]), where t is the effective intersite hopping integral and $\Delta_{s.f.}$ is the energy splitting between occupied and unoccupied states with different spin projections, which is proportional to the Stoner I in LSDA but much larger in LSDA+U, due to the corrections due to U [48]. This as well as the reduction of t value, caused by the localization, leads to an overall suppression of the J_{ij}. A clearer overview of this reduction can be obtained by looking at Table I.

In Table I, we present the spin moment as well as the total and orbital-decomposed J_{ij}'s between the nearest Mn atoms. The total value obtained in LSDA+U is in good agreement with the experimental value of 0.485 mRy [46]. Concerning the orbital decomposition, we note that the e_g-derived contributions are practically negligible, since these states are almost empty and therefore do not participate in the exchange interactions. On the contrary, the $t_{2g} - t_{2g}$ contribution is decisive for the general magnetic behavior of the system and gives rise to the G-type AFM order. There is also a small $e_g - t_{2g}$ term, which appears due to a nonperfect relative alignment of the neighboring MnO_6 octahedra.

Finally, we calculated the ordering temperature (T_N) of bulk CMO by means of classical MC simulations. We obtained 285 and 150 K in LSDA and LSDA+U, respectively. Our LSDA value is in good agreement with the value of 434 K obtained in Ref. [45] by means of the mean-field approximation, which usually overestimates the ordering temperature. The experimental ordering temperature is around 120 K [13,14], which is very close to the LSDA+U estimate. Overall, the obtained results indicate that the LSDA+U calculation with $U = 4$ eV provides an accurate description of the magnetic properties of bulk CMO, as compared with experimental data. Therefore, in the following, we will focus especially on LSDA+U when addressing the CMO slabs.

TABLE I. Calculated spin moments of Mn atoms (in μ_B) as well as total and orbital-decomposed J_{ij}'s (in mRy) between NNs in bulk CMO.

	M_s	Total	e_g-e_g	t_{2g}-t_{2g}	e_g-t_{2g}
LSDA	2.31	− 0.786	0.018	− 1.096	0.291
LSDA+U	2.55	− 0.495	− 0.002	− 0.646	0.153
LSDA-ASW[a]	2.44	− 0.704			
LSDA[b]	2.36	− 1.911			
Expt.[c]		− 0.485			

[a]Ref. [45].
[b]Ref. [18].
[c]Ref. [46].

B. Results for the slab

1. Unrelaxed slab

First, we considered an unrelaxed freestanding slab of CMO as a truncated bulk structure. As illustrated in Fig. 3, the slab is terminated by layers of MnO_2 from both sides. The thickness (see Sec. II) was determined by comparing the spin moment of the Mn atom in the innermost layer with the bulk value. This difference was found to be less than 0.2%, which indicated that the considered slab thickness is sufficient to avoid spurious interactions between the two surface layers.

In Fig. 2, the DOS of the surface, subsurface, and innermost (middle) layers of the unrelaxed CMO slab are presented. In both LSDA (not shown here) and LSDA+U (see Fig. 2), surface and subsurface layers are metallic, while the middle layer is insulating, similarly to the bulk. This is a consequence of the broken symmetry at the surface, which leads to a different crystal field acting on the Mn d states, as also observed in other TM perovskites [49]. As a consequence, d_{z^2} states appear at E_F, leading to metallic character. In LSDA+U, this metallicity is strongly quenched, with respect to LSDA, but still present.

Filippetti and Pickett [18] reported that the ground state for the slab of CMO is basically a G-type AFM, except that for the surface atoms, the spin moments are flipped such that each atom at the surface is coupled with the atom in the subsurface ferromagnetically (see bottom panel of Fig. 3). In other words, a SF occurs for the surface Mn atoms. We therefore investigated the electronic structure of the CMO slab for the G-type AFM, with and without a SF at the surface. For simplicity, we refer to the former as the AFM configuration and to the latter as the SF configuration. Comparing the total energies of these states, our results for the unrelaxed slab are in good agreement with those of Ref. [18], showing the SF configuration as ground state, being 78 (22) meV lower in total energy than the AFM configuration in LSDA (LSDA+U).

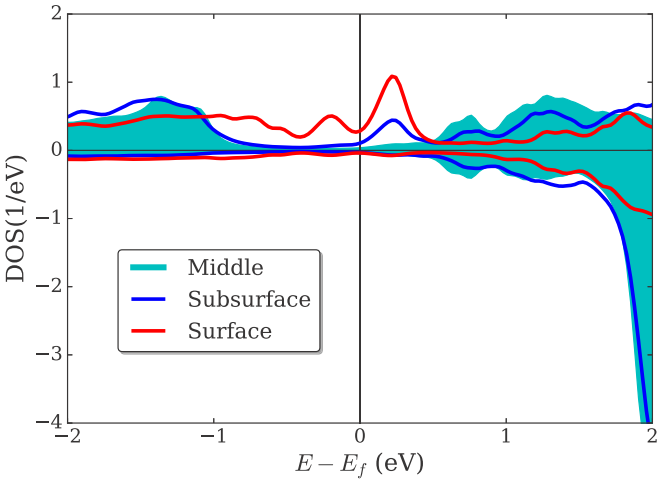

FIG. 2. The Mn-projected DOS of the unrelaxed structure of CMO slab in the SF configuration for the majority- and minority-spin components obtained in LSDA+U.

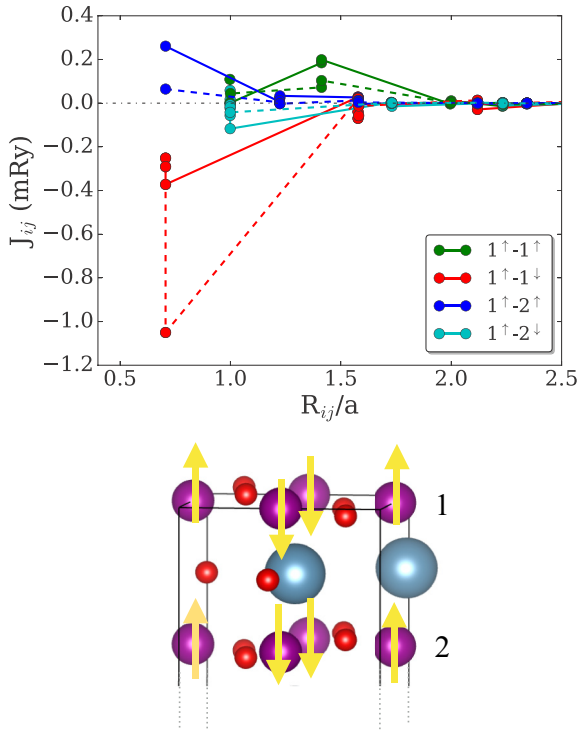

FIG. 3. Top panel: The exchange interaction between an atom at the surface of CMO with the atoms at the surface (layer 1) and subsurface (layer 2) in LSDA (solid lines) and LSDA+U (dashed lines) for an unrelaxed slab. Bottom panel: The obtained ground-state magnetic configuration for the unrelaxed surface of CMO. The purple balls represent Mn atoms, with the yellow arrow indicating the spin magnetization direction; the red balls are O and the blue ones are Ca atoms.

Using the SF configuration as the reference state, the exchange parameters between the atoms at the surface and the subsurface were calculated. The results are shown in Fig. 3, where surface atoms are labeled as 1 and subsurface atoms as 2. The exchange parameters between the atoms in the inner layers are not shown, since they are very similar to the results for the bulk, illustrated in Fig. 1(b). The most interesting observation is that the coupling of the atom at the surface and the one right below at the subsurface is FM (see the blue lines). In addition, the AFM coupling between the closest Mn atoms at the surface is also observed (red lines), although it is substantially weaker than that in the bulk. These two observations confirm the SF scenario at the surface, which was obtained in Ref. [18] by total-energy comparison.

Usually the J_{ij}'s obtained by means of magnetic force theorem depend on the magnetic configuration they are extracted from. It is important to verify that the reference state corresponds to the ground state. It is also interesting, however, to calculate the J_{ij}'s from the G-type AFM order without the surface SF. These results indicated an instability of this state, suggesting that the SF scenario is the ground state. Thus, we can claim that the results provided by all different methods offer a robust physical picture and point at the same conclusion.

The SF configuration can be explained by looking at the electronic structure. The metallicity of surface and subsurface layers in CMO is due the presence of the d_{z^2} states at the Fermi surface. These orbitals point towards each other, which facilitates electron hopping between the Mn ions through a double-exchange-like mechanism and provides a FM coupling. This result, in the limit of LSDA, has also been observed in several prior studies [23,44].

An interesting feature of Fig. 3 is that LSDA+U predicts larger values for the exchange parameters (red dashed line), in contrast to our conclusion for the bulk, where LSDA+U suppressed the LSDA exchange. This can be explained in terms of the metallicity of the surface layer [50]. In general, the exchange interactions in manganites can be regarded as the combination of ferromagnetic double-exchange and antiferromagnetic superexchange interactions. The superexchange interactions are inversely proportional to U and, therefore, weaker in LSDA+U. The double exchange is, on the other hand, proportional to the transfer integral and (to a first approximation) does not depend on U. In the bulk, the superexchange dominates and therefore one expects the observed scaling. At the surface, instead, the metallic character drastically changes the behavior of the magnetic interactions and the argument based solely on the analysis of the superexchange strength is no longer valid. These are general trends, but one should keep in mind that in LSDA+U, there are also other factors (e.g., the oxygen states), which can alter this conclusion.

Overall, our results for the CMO surface illustrate that the sign of the magnetic interaction between Mn ions is very sensitive to their local atomic environment. This stimulated us to study how the magnetic properties vary once the reconstruction of the surface geometry is taken into account in *ab initio* simulations.

2. *The effect of geometry relaxation*

We performed geometry relaxation for two different spin configurations of the slab at the surface, i.e., AFM and SF. Once relaxation is taken into account, the magnetic ground state of the CMO slab corresponds to the AFM configuration, in contrast to the unrelaxed slab, where the SF configuration had a lower total energy. This can likely be explained by looking at the DOS. In LSDA, both configurations give a metallic solution at the surface, but with a smaller DOS at E_F than for the unrelaxed structure (not shown). In LSDA+U, instead, the surface in the AFM configuration becomes an insulator with a band gap of 0.4 eV, as shown in Fig. 4. The insulating character at the surface holds also for the SF configuration, as reported in Fig. 5, for the sake of comparison. In light of these results, it is tempting to assign the change of the sign of the magnetic interaction to the suppression of the double-exchange mechanism, which is accompanied with a decrease (or even removal) of the metallicity.

The exchange parameters of the AFM configuration in LSDA+U are reported in Fig. 6. These results also confirm that the SF of the surface atoms disappears after the geometry relaxation (see the blue lines). This conclusion is obtained both in the LSDA and in the LSDA+U methods. Moreover, additional calculations using the SF configuration as the

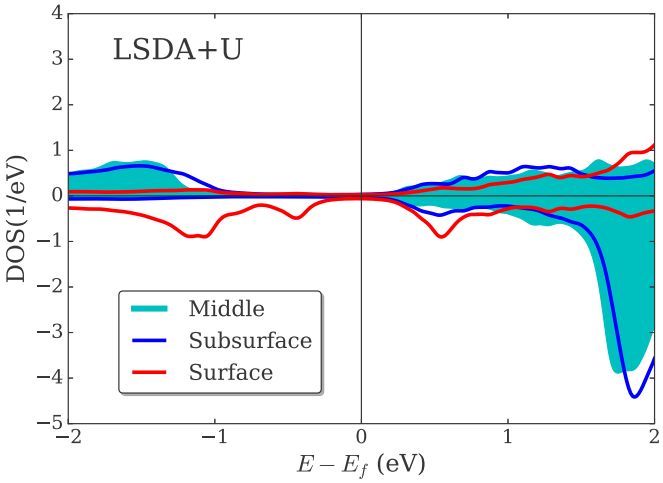

FIG. 4. The Mn-projected DOS of the relaxed structure of a CMO slab in the AFM configuration for the majority- and minority-spin components obtained in LSDA+U.

reference state also lead to the same conclusion. These results (not shown here) are qualitatively very similar to the ones shown in Fig. 6, but with minor differences in their magnitudes. For instance, in LSDA+U, the NN exchange parameter between the atom at the surface and the subsurface is about -0.35 m Ry, while the corresponding parameter in Fig. 6 is equal to -0.42 m Ry. Overall, our findings seem very robust and not related to the reference state.

3. *Electron doping*

An excess of electrons can appear in CMO due to doping or they can emerge spontaneously due to the presence of oxygen vacancies. This can influence the magnetic properties and therefore we have examined how the electron doping affects the J_{ij}'s at the surface. For this purpose, we have performed an additional set of calculations varying the chemical potential of the system. Since the converged DFT+ potential has not been modified, one can best describe this procedure as that the doping was simulated within a rigid-band model. Note that the present approach is extremely simplified and assumes a uniform distribution of an additional negative charge in the system. Most importantly, it neglects structural changes leading to the electron trapping, i.e., the formation of magnetic polarons [10]. Nonetheless, the aim of these simulations is to provide a qualitative picture about the sensitivity of the obtained preferable magnetic order to the stoichiometry of the system.

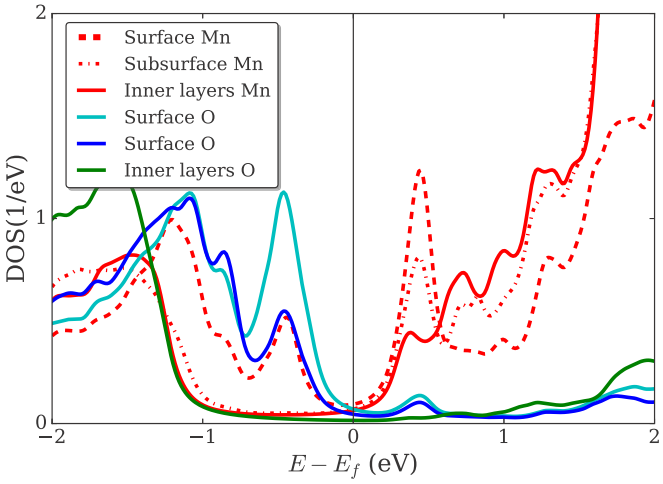

FIG. 5. Projected DOS for Mn $3d$ and oxygen $2p$ orbitals calculated in the SF configuration after geometrical relaxation within LSDA+U.

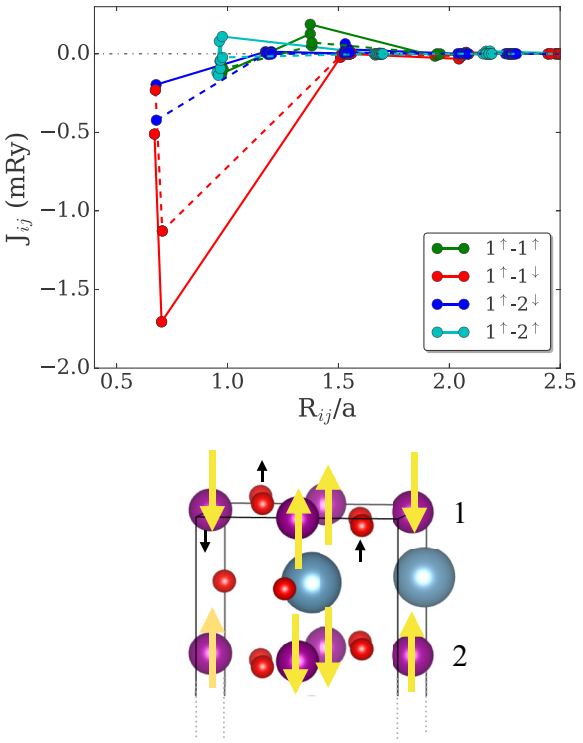

FIG. 6. Top panel: The exchange interaction between an atom at the surface of CMO and the atoms at the surface (layer 1) and subsurface (layer 2) in LSDA (solid lines) and LSDA+U (dashed lines) for a relaxed slab. Bottom panel: The obtained magnetic order for the relaxed structure. The purple balls represent Mn atoms with the yellow arrow indicating spin direction. The black arrows indicate the direction of the atomic displacement after geometry relaxation.

Figure 7 shows the dependence of the most relevant magnetic couplings at the surface of CMO on electron doping. The NN exchange interaction between two atoms at the surface is indicated by two different arguments $J_{1\uparrow 1\downarrow}$ and $J'_{1\uparrow 1\downarrow}$. As mentioned before, this is because of the orthorhombic structure of CMO which makes the x and y axes inequivalent and therefore the distance between the Mn atoms in one direction is 0.17 Å shorter than the other one. The interaction between the atom at the surface and the one right below in the subsurface is indicated by $J_{1\uparrow 2\downarrow}$, as also depicted in the bottom panel of Fig. 6. One can see that the interactions between Mn atoms at the surface are relatively robust with respect to the shift of the chemical potential. In the entire range of doping levels considered here, these couplings remain AFM. On the other hand, the surface-subsurface interaction ($J_{1\uparrow 2\downarrow}$), being AFM for low doping, changes its sign when more than 0.04 electrons

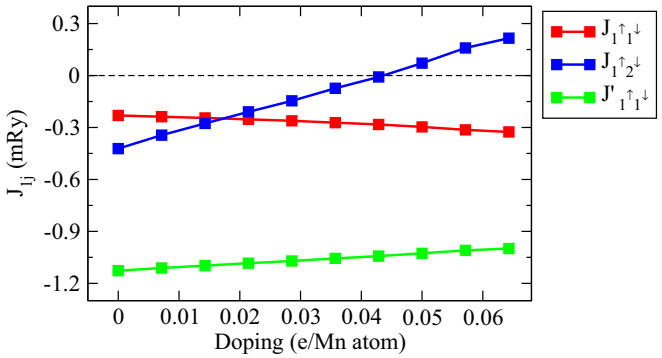

FIG. 7. The NN exchange parameter as a function of electron doping in the relaxed structure of a CMO slab. $J_{1\uparrow 1\downarrow}$ and $J'_{1\uparrow 1\downarrow}$ indicate the exchange interactions between two atoms at the surface and $J_{1\uparrow 2\downarrow}$ is the exchange between the atom at the surface and the one at the subsurface.

per Mn atom are added to the system. More long-ranged interactions between the surface and subsurface atoms are also ferromagnetic (data not shown). At this point, the SF of Mn spins is expected to take place at the surface of CMO and, consequently, a ferromagnetic coupling between surface and subsurface atoms appears.

IV. CONCLUSIONS

In this paper, we have analyzed the magnetic properties of the bulk and surface of CMO. We found that the bulk is well described in LSDA+U calculations, a conclusion that had been pointed out in the past, e.g., in Refs. [51,52]. This conclusion is based on the fact that theoretical exchange interactions combined with an effective spin Hamiltonian result in a Néel temperature that is in agreement with observations. In the bulk, we find that the $t_{2g} - t_{2g}$ superexchange channel is the dominating exchange mechanism.

For the surface of CMO, we find that structural relaxations play an important role and that when taken into account, the (001) surface of CMO has the same AFM ordering as the bulk. Our results indicate a large exchange striction in which small structural displacements provide a significant modification of the interatomic exchange interaction, even to the extent that the sign changes. Finally, we predict that a small amount of electron doping of 0.04 electrons per Mn atom can cause a SF transition of the Mn surface atoms. It would be interesting to verify this prediction in experiments and we hope that such investigation will be carried out in the future.

ACKNOWLEDGMENTS

The authors are grateful to Stefan Blügel (Forschungszentrum Jülich) for stimulating discussions. O.E. acknowledges support from the Swedish Research Council (VR), eSSENCE and the KAW Foundation. The work of I.V.S. is partly supported by a grant of Russian Science Foundation (Project No. 14-12-00306). The computer simulations are performed on computational resources provided by NSC and UPPMAX allocated by the Swedish National Infrastructure for Computing (SNIC). D.C.M.R. acknowledges CAPES (Brazil).

[1] E. Dagotto, *Nanoscale Phase Separation and Colossal Magnetoresistance: The Physics of Manganites and Related Compounds*, Springer Series in Solid-State Sciences (Springer, Berlin, 2013).
[2] B. Sanyal and O. Eriksson, *Advanced Functional Materials: A Perspective from Theory and Experiment*, Science and Technology of Atomic, Molecular, Condensed Matter & Biological Systems (Elsevier Science, New York, 2012).
[3] S. Bhattacharjee, E. Bousquet, and P. Ghosez, Phys. Rev. Lett. **102**, 117602 (2009).
[4] S.-W. Cheong and M. Mostovoy, Nat. Mater. **6**, 13 (2007).
[5] P. Schiffer, A. P. Ramirez, W. Bao, and S.-W. Cheong, Phys. Rev. Lett. **75**, 3336 (1995).
[6] N. Reyren, S. Thiel, A. D. Caviglia, L. F. Kourkoutis, G. Hammerl, C. Richter, C. W. Schneider, T. Kopp, A.-S. Rüetschi, D. Jaccard, M. Gabay, D. A. Muller, J.-M. Triscone, and J. Mannhart, Science **317**, 1196 (2007).
[7] A. Ohtomo and H. Hwang, Nature (London) **427**, 423 (2004).
[8] W. Meevasana, P. D. C. King, R. H. He, S.-K. Mo, M. Hashimoto, A. Tamai, P. Songsiriritthigul, F. Baumberger, and Z.-X. Shen, Nat. Mater. **10**, 114 (2011).
[9] A. P. Ramirez, P. Schiffer, S.-W. Cheong, C. H. Chen, W. Bao, T. T. M. Palstra, P. L. Gammel, D. J. Bishop, and B. Zegarski, Phys. Rev. Lett. **76**, 3188 (1996).
[10] J. J. Neumeier and J. L. Cohn, Phys. Rev. B **61**, 14319 (2000).
[11] P. Barone, D. Di Sante, and S. Picozzi, Phys. Rev. B **89**, 144104 (2014).
[12] P. W. Anderson, Phys. Rev. **115**, 2 (1959).
[13] N. N. Loshkareva, L. V. Nomerovannaya, E. V. Mostovshchikova, A. A. Makhnev, Y. P. Sukhorukov, N. I. Solin, T. I. Arbuzova, S. V. Naumov, N. V. Kostromitina, A. M. Balbashov, and L. N. Rybina, Phys. Rev. B **70**, 224406 (2004).
[14] Z. Zeng, M. Greenblatt, and M. Croft, Phys. Rev. B **59**, 8784 (1999).
[15] C. Zener, Phys. Rev. **82**, 403 (1951).
[16] P. G. de Gennes, Phys. Rev. **118**, 141 (1960).
[17] P. W. Anderson and H. Hasegawa, Phys. Rev. **100**, 675 (1955).
[18] A. Filippetti and W. E. Pickett, Phys. Rev. Lett. **83**, 4184 (1999).
[19] V. I. Anisimov, F. Aryasetiawan, and A. I. Lichtenstein, J. Phys. Condens. Matter **9**, 767 (1997).
[20] G. Kresse and D. Joubert, Phys. Rev. B **59**, 1758 (1999).
[21] G. Kresse and J. Furthmüller, Comput. Mater. Sci. **6**, 15 (1996).
[22] J. P. Perdew and Y. Wang, Phys. Rev. B **45**, 13244 (1992).
[23] A. Filippetti and W. E. Pickett, Phys. Rev. B **62**, 11571 (2000).
[24] J. Hong, A. Stroppa, J. Íñiguez, S. Picozzi, and D. Vanderbilt, Phys. Rev. B **85**, 054417 (2012).
[25] J. H. Jung, K. H. Kim, D. J. Eom, T. W. Noh, E. J. Choi, J. Yu, Y. S. Kwon, and Y. Chung, Phys. Rev. B **55**, 15489 (1997).
[26] U. Aschauer, R. Pfenninger, S. M. Selbach, T. Grande, and N. A. Spaldin, Phys. Rev. B **88**, 054111 (2013).

[27] I. V. Solovyev, P. H. Dederichs, and V. I. Anisimov, Phys. Rev. B **50**, 16861 (1994).
[28] J. M. Wills, M. Alouani, P. Andersson, A. Delin, O. Eriksson, and O. Grechnyev, in *Full-Potential Electronic Structure Method*, edited by E. S. H. Dreysse, Springer Series in Solid-State Sciences, (Springer-Verlag, Berlin, 2010).
[29] A. Grechnev, I. Di Marco, M. I. Katsnelson, A. I. Lichtenstein, J. Wills, and O. Eriksson, Phys. Rev. B **76**, 035107 (2007).
[30] O. Grånäs, I. Di Marco, P. Thunström, L. Nordström, O. Eriksson, T. Björkman, and J. M. Wills, Comput. Mater. Sci. **55**, 295 (2012).
[31] I. Di Marco, J. Minár, S. Chadov, M. I. Katsnelson, H. Ebert, and A. I. Lichtenstein, Phys. Rev. B **79**, 115111 (2009).
[32] A. I. Liechtenstein, M. I. Katsnelson, V. P. Antropov, and V. A. Gubanov, J. Magn. Magn. Mater. **67**, 65 (1987).
[33] Y. O. Kvashnin, O. Grånäs, I. Di Marco, M. I. Katsnelson, A. I. Lichtenstein, and O. Eriksson, Phys. Rev. B **91**, 125133 (2015).
[34] B. Skubic, J. Hellsvik, L. Nordström, and O. Eriksson, J. Phys.: Condens. Matter **20**, 315203 (2008).
[35] S. Khmelevskyi, T. Khmelevska, A. V. Ruban, and P. Mohn, J. Phys: Condens. Matter **19**, 326218 (2007).
[36] J. Rusz, L. Bergqvist, J. Kudrnovský, and I. Turek, Phys. Rev. B **73**, 214412 (2006).
[37] A. Jacobsson, B. Sanyal, M. Ležaić, and S. Blügel, Phys. Rev. B **88**, 134427 (2013).
[38] I. V. Solovyev and K. Terakura, Phys. Rev. B **58**, 15496 (1998).
[39] I. V. Solovyev, Phys. Rev. B **74**, 054412 (2006).
[40] I. V. Solovyev, Phys. Rev. B **87**, 144403 (2013).
[41] H. Y. Hwang, S.-W. Cheong, N. P. Ong, and B. Batlogg, Phys. Rev. Lett. **77**, 2041 (1996).
[42] H. B. Peng, B. R. Zhao, Z. Xie, Y. Lin, B. Y. Zhu, Z. Hao, H. J. Tao, B. Xu, C. Y. Wang, H. Chen, and F. Wu, Phys. Rev. Lett. **82**, 362 (1999).
[43] J. Zaanen, G. A. Sawatzky, and J. W. Allen, Phys. Rev. Lett. **55**, 418 (1985).
[44] T. T. Nguyen, T. C. Bach, H. T. Pham, T. T. Pham, D. T. Nguyen, and N. N. Hoang, Phys B: Condens. Matter **406**, 3613 (2011).
[45] C. Cardoso, R. P. Borges, T. Gasche, and M. Godinho, J. Phys. Condens. Matter **20**, 035202 (2008).
[46] C. Domb, M. Green, and J. Lebowitz, *Phase Transitions and Critical Phenomena*, Phase Transitions and Critical Phenomena (Academic, New York, 1984), Vol. 9.
[47] I. I. Mazin, Phys. Rev. B **75**, 094407 (2007).
[48] V. I. Anisimov, J. Zaanen, and O. K. Andersen, Phys. Rev. B **44**, 943 (1991).
[49] C. Autieri, J. Phys. Condens. Matter **28**, 426004 (2016).
[50] I. V. Solovyev and K. Terakura, Phys. Rev. Lett. **82**, 2959 (1999).
[51] F. F. Fava, P. D'Arco, R. Orlando, and R. Dovesi, J. Phys. Condens. Matter **9**, 489 (1997).
[52] A. J. Millis, Phys. Rev. B **55**, 6405 (1997).